Revised manuscript (clean version) Click here to view linked References

Protein-folding-inspired approach for UF fouling mitigation using elevated membrane cleaning temperature and residual hydrophobic-modified flocculant after flocculation-sedimentation pre-treatment

Zhangzheng Wang [a], Ruhui Chen [a], Yunyun Li [a], Weiben Yang [a], Ziqi Tian [c], Nigel J. D. Graham [b], Zhen Yang [a,*]

[a] School of Chemistry and Materials Science, Jiangsu Provincial Key Laboratory of Material Cycling and Pollution Control, Nanjing Normal University, Nanjing 210023, China

[b] Department of Civil and Environmental Engineering, Imperial College London, SW7 2AZ, UK

[c] Ningbo Institute of Materials Technology & Engineering, Chinese Academy of Sciences, Ningbo 315000, China

[*] Corresponding author. E-mail: yangzhen@njnu.edu.cn

Abstract: Hydrophobic-modified flocculants have demonstrated considerable promise in the removal of emerging contaminants by flocculation. However, there is a lack of information about the impacts of dosing such flocculants on the performance of subsequent treatment unit(s) in the overall water treatment process. In this work, inspired by the ubiquitous protein folding phenomenon, an innovative approach using an elevated membrane cleaning temperature as the means to induce residual hydrophobic-modified chitosan flocculant (TRC), after flocculation-sedimentation, to reduce membrane fouling in a subsequent ultrafiltration was proposed; this was evaluated in a continuous flocculation-sedimentation-ultrafiltration (FSUF) process treating samples of the Yangtze River. The hydrophobic chains of TRC had similar temperature-dependent hydrophobicity to those of natural proteins. In the 40-day operation of the FSUF system with combined dosing of alum and TRC, a moderately elevated cleaning water temperature (45 ^{o}C) of both backwash with air-bubbling and soaking with sponge-scrubbing cleaning, significantly reduced reversible and irreversible fouling resistance by 49.8%~61.3% and 73.9%~83.3%, respectively, compared to the system using cleaning water at 25 ^{o}C. Material flow analysis, statistical analysis, instrumental characterizations, and computational simulations, showed that the enhanced fouling mitigation originated from three factors: the reduced contaminant accumulation onto membranes, the strengthened membrane-surface-modification role of TRC, and the weakened structure of the fouling material containing TRC, at the elevated cleaning temperature. Other measures of the performance, these being water purification, membrane stability and economic aspects, also confirmed the potential and feasibility of the proposed approach. This work has provided new insights into the role of hydrophobic-modified flocculants in membrane fouling control, in addition to emerging contaminant removal, in a FSUF surface water treatment process.

Keywords: Hydrophobic-modified flocculant; Membrane cleaning temperature; Fouling control; Surface water treatment; Flocculation; Ultrafiltration

1. Introduction

The contamination of surface water used for drinking water sources, by either conventional or emerging contaminants, has continued to increase and poses a serious threat to drinking water security (Larsen et al., 2016). Improved drinking water treatment technologies, as a response, are continuously being developed. Among them, the flocculation-sedimentation-ultrafiltration (FSUF) hybrid process train, has the merits of a compact continuous treatment flow, simple operation and maintenance, no secondary pollution risk of contaminant degradation (e.g. by oxidation), relatively low cost, and high treated water quality. As such, it has attracted considerable attention and been applied in many drinking water treatment plants (DWTPs) (Gan et al., 2021; Long et al., 2021). In the FSUF process, the flocculation-sedimentation (FS), prior to UF, acts as an efficient pretreatment to reduce membrane-fouling-causing contaminants, involving inorganic suspended solids (ISS) and natural organic matter (NOM) (Ma et al., 2014); in addition, unsettled residual micro-flocs (i.e. flocculant-contaminant complexes) after sedimentation, can be effectively retained by UF, which gives rise to an improved quality of the produced water (Liu et al., 2017).

Despite the above synergistic effects between FS and UF, the application of the combined process still has shortcomings that require improvement, with regard to current and future concerns in water treatment. One of the most enduring challenges for all kinds of membrane-filtration-based technologies, is membrane fouling control (Xu et al., 2021). FS pretreatment alone has been found to be insufficiently effective for fouling mitigation during the long-term running of FSUF (Su et al., 2021). The

accumulation of residual flocculants (especially those with high molecular weight (MW) (He et al., 2021)), as well as micro-flocs, on the membrane may induce or aggravate fouling, leading to unavoidable flux decline and increased operating cost (Xu et al., 2021). Therefore, alternative approaches, involving membrane surface modification and optimization of operation process (such as membrane cleaning methods) (Guo et al., 2021; Li et al., 2022), have been proposed for fouling control.

In recent years, there has been increasing concern in the drinking water supply industry about the contamination of source waters by emerging organic contaminants (EOCs, such as the well-known anthropogenic antibiotics) (Wilkinson et al., 2017), and how to effectively remove the EOCs by the well-established FSUF process in existing DWTPs (Yang et al., 2022). Conventional flocculants (either organic (e.g. polyacrylamide (PAM) and its derivatives) or inorganic (e.g. Al or Fe salts)), despite their high performance for ISS and NOM removal, have been shown to be ineffective for the removal of small-sized antibiotic molecules (Demissie et al., 2021). To address this, a promising approach, recently reported, is to develop new flocculants through chemical modification of conventional hydrophilic flocculants (for example: chitosan, metal hydroxides, etc.) with moderately hydrophobic organic chains (Demissie et al., 2021; Liu et al., 2019; Wang et al., 2022; Yang et al., 2020). By doing so, the hydrophobic association between the hydrophobic-modified flocculants and small antibiotic molecules can be strengthened (Liu et al., 2019; Wang et al., 2022; Yang et al., 2020), thereby enabling greater binding of antibiotics into floc particles during flocculation, and removal by subsequent sedimentation.

The benefit of strengthening the hydrophobicity of flocculants dosed in the flocculation unit is not only that it can increase the water purification capacity (enhancing the treatment efficacy for EOC removal) as reported (Liu et al., 2019; Wang

et al., 2022; Yang et al., 2020; Yang et al., 2021), but also that it may increase other aspects of performance, in particular, the formation (during filtration) and destruction (during membrane cleaning) of foulant materials on the membrane surface in the subsequent UF unit (Ho et al., 2022). This latter aspect has not been fully studied as yet, and is inspired by the ubiquitous protein folding phenomenon in nature (Colvin et al., 2016; Dill et al., 2008). As has been acknowledged, water-mediated hydrophobic association plays a vital role in protein folding, through which tertiary and quaternary structures of proteins with mature functions are achieved (Eisenberg and Sawaya, 2016). The apolar segments of proteins form hydrophobic cores, whereas the polar and charged chains make up the stabilized water-exposed surface of proteins (Walti et al., 2016). Similarly, it is suggested that the hydrophobic chains of the residual hydrophobic-modified flocculants after FS be tightly bound onto the hydrophobic surface of ultrafiltration membranes (such as the commonly used polyvinylidene fluoride (PVDF) membranes) through hydrophobic association, whereas the hydrophilic and charged chains of flocculants form a stabilized water-exposed surface. In this way, residual hydrophboic-modifed flocculants after FS, exert a surface-modification effect on UF membrane which can provide a protective hydration layer on the membrane surface to inhibit fouling formation.

Although a part of the residual hydrophobic-modified flocculants will participate in the above-proposed in-situ membrane surface modification, another part will become involved in influencing the nature of the fouling (Li and Elimelech, 2004) on the used membrane. Inspired by the structural changes of proteins with the variation of temperature (Wolfenden et al., 2015), structure of fouling deposits containing hydrophobically modified flocculants may also change at different temperatures. This may bring about new opportunities for developing more efficient membrane cleaning

115 modes (e.g. by adjusting the cleaning water temperature). By revisiting the features of
116 protein folding, it was recognized that the strength of hydrophobic association is
117 temperature-dependent; thus, with the rise of temperature, the hydrophobicity of most
118 of the hydrophobic chains in proteins increases and the original stable tertiary or
119 quaternary structure of proteins may be weakened) (Baldwin, 1986; Wolfenden et al.,
120 2015). Based on this, it was hypothesized that the temperature-responsive characteristic
121 of hydrophobic chains could possibly be utilized for the destruction of membrane
122 fouling by an environmental-benign and chemical-free membrane cleaning method.
123 Thus, as residual hydrophobic-modified flocculants enter the inside of the membrane
124 fouling layer, and act as one of the building materials, increasing the cleaning water
125 temperature may induce the flocculants to decrease the stability of the fouling structure
126 from within, promoting the release of material under turbulence caused by the
127 backwash with air-bubbling, soaking with scrubbing, or other techniques. However,
128 little information is known about this approach for membrane cleaning and fouling
129 control in the continuous-flow FSUF process with the dosing of hydrophobic-modified
130 flocculants.

131 In this work, the hypothesis of using membrane cleaning temperature as the means
132 of reducing fouling, in the long-term operation of a continuous-flow FSUF process with
133 the dosing of hydrophobic-modified flocculant, was evaluated for the first time. To
134 achieve this, laboratory experiments were carried out: raw water samples collected from
135 the Yangtze River were employed; chitosan modified with thermo-responsive
136 hydrophobic chains (denoted as TRC), as well as commercial alum and PAM for
137 comparison, was selected as the flocculant; both backwash with air-bubbling (B&A
138 cleaning) and soaking with sponge-scrubbing (S&S cleaning) were employed for
139 membrane cleaning, and the effects of the B&A and S&S cleaning temperatures on

fouling control were studied; the underlying mechanisms of fouling reduction were clarified with evidence from material flow analysis, statistical analysis, instrumental characterizations, and computational simulations. The results of this work present a new, proof-of-concept approach to the control of membrane fouling in the FSUF process, and are expected to provide new insights into the role of hydrophobic-modified flocculants in surface water treatment.

2. Materials and methods

2.1. Water samples and flocculants

Raw water from the Yangtze River was sampled in August, 2021, at Caishi DWTP, Ma'anshan City, Anhui Province, China (Supporting Information (SI) Fig. S1). To represent micro-polluted surface water contaminated by trace antibiotics, the samples were spiked with stock solutions of four commonly detected antibiotics (sulfamethoxazole (SMX), norfloxacin (NOR), tetracycline (TC) and roxithromycin (ROX); Dalian Meilun Biotechnol. Co., Dalian, Liaoning Province, China; physicochemical parameters in the SI, Table S1), to reach a concentration of 0.1 μg/L of each, before the water treatment tests. Water quality parameters are listed in Table 1.

The hydrophobic-modified flocculant TRC, with optimized structural parameters (as shown in Fig. 1a) according to the authors' previous work (Wang et al., 2022), was synthesized by grafting thermo-responsive hydrophobic chains (poly(N-iso-propylacrylamide), PNIPAM) onto chitosan (viscosity-average MW: 820 kDa; deacetylation degree: 86%; Shandong Aokang Biotechnol. Co., Jinan, Shandong Province, China). The detailed synthesis method, as well as characterization results, are given in the SI (Text S1 and Fig. S2). Alum and PAM were purchased from Nanjing Chem. Reagent Co., Nanjing, Jiangsu Province, China.

2.2. Water treatment tests

Continuous-flow FSUF tests were conducted using a parallel continuous-flow apparatus (schematic description of the experimental set-up shown in Fig. 1b) at 25 ℃ for 40 days, to evaluate the performance of membrane fouling control and water purification. The flow rate was maintained at 12 L/day throughout.

The flocculant/coagulant dosages used in the FSUF process tests were optimized by preliminary jar tests (operation details in the SI, Text S2); the results of jar tests (removal efficiencies (REs)-dosage profiles depicted in the SI, Fig. S3) were consistent with those reported in previous literature (Melo-Guimaraes et al., 2013; Demissie et al., 2021). Neither alum nor PAM could effectively remove trace antibiotics, but TRC exhibited improved REs for both conventional parameters (RE(turbidity) and RE(DOC): ~90%) and trace antibiotics (REs: 72%-92%), compared to alum and PAM. Successive dosing of the inorganic alum (6 mg/L) and organic TRC (4 mg/L) demonstrated enhanced cost-effectiveness by increasing the REs and decreasing the optimal dosages of TRC. As alum was effective in the removal of conventional contaminants (ISS and NOM), this enabled TRC, dosed subsequently, to be used where it was most effective (for antibiotic removal) (Wang et al., 2022).

The corresponding optimal dosages of flocculant/coagulant were dosed in the first flocculation tank. The mechanical stirring speeds of the four flocculation tanks were 200, 150, 100 and 50 rpm, as shown in Fig. 1b, respectively. The hydraulic retention time (HRT) of each flocculation tank, the inclined plate sedimentation tank, and the submerged UF tank were 5, 60, and 30 min, respectively. A cluster of PVDF hollow fiber UF membranes (Hangzhou Haotian Co., Hangzhou, Zhejiang Province, China), with pore size of 20 nm, surface area of 0.025 m^2, and inner/outer diameter of 1.0/1.4

mm, were employed in the UF tank. B&A cleaning, involving backwash (0.66 L/(m^2·min)) accompanied with air-bubbling (2.5 L/min) for 1 min, was performed after every 0.5-h of operation; S&S cleaning, by soaking the membrane in water for 5 min accompanied with sponge-scrubbing (details provided in the SI, Text S3), was performed after every 13-day period. In addition to cleaning at 25 ^{o}C, a reduced (5 ^{o}C) and an elevated (45 ^{o}C) temperature, representing a relatively significant difference, were also tested for both B&A and S&S cleaning, to investigate the effects of cleaning temperatures on fouling control as proposed above. Considering the aspects of energy consumption (which increases with temperature elevation above ambient) and microorganism growth (which can be inhibited at a temperature above the normal maximum temperature for the process-related microorganisms), the elevated temperature selected in the cleaning tests was 45 ^{o}C. This temperature could be facilely achieved using industrial low-grade waste heat via a heat exchanger, if the concept of using elevated cleaning temperature for fouling control was to be promoted to large-scale practical applications (Adhikary et al., 2020; Zhou et al., 2015). Membrane fouling, represented by trans-membrane pressure (TMP), was monitored. Reversible (REV, m^{-1}) and irreversible fouling resistances (IRR, m^{-1}), defined as the related material that is able, or unable, to be removed by the S&S cleaning, respectively, were calculated according to equations (Eqs.) 1 and 2 (Guo et al., 2021):

$$REV = (TMP_b - TMP_a)/(\mu \cdot J) \quad \text{(Eq. 1)}$$

$$IRR = (TMP_a - TMP_0)/(\mu \cdot J) \quad \text{(Eq. 2)}$$

where TMP_0, TMP_b, and TMP_a (Pa) are the TMP values at the beginning of the testing (day 0), before, and after, S&S cleaning, respectively; μ is the viscosity (Pa·s) of water; and J (m^3/m^2·s) is the flux.

Water quality parameters of the effluents after the fourth flocculation tank, the

sedimentation tank, and the UF tank, respectively, were continuously measured every day (detailed methods provided in the SI, Text S4). Among them, the concentrations of TRC were determined by a fluorescent labeling technique. Details of the technique, as well as its feasibility verification, are provided in the SI, Text S4 and Figs. S4-S7. To exclude the impact of material adsorption onto the inner surface of the FSUF apparatus, controlled experiments were conducted to calibrate the results; each data point was the average from three parallel experiments.

2.3. Material flow analysis (MFA), statistical analysis, instrumental characterizations, and computational simulations

MFA, to summarize the main material path, was carried out using Sankey diagrams (Graedel, 2019; Van Vuuren et al., 2019). Principal component analysis (PCA) and correlation analysis of the MFA results were conducted using IBM SPSS® Statistics 20 software. Details of analytical instruments and methods, involving measurements of water contact angles (WCAs), zeta potentials (ZPs) and sizes of TRC, SEM and AFM observations, fouling cake layer thickness determination, mechanical property tests, pore size distribution analysis, and measurements of floc size and fractal dimension (D_F, representing the compactness of porous materials), are described in the SI (Text S4, S5 and Fig. S8). Computational simulations of molecular structures and the corresponding binding energies of different molecular pairs were performed using Materials Studio® 2019 software (Chen et al., 2019; Liu et al., 2019) with detailed information provided in the SI, Text S6.

3. Results and discussion

3.1 Thermo-responsiveness of TRC

The thermo-responsiveness of the hydrophobic-modified flocculant is the key premise of the above-hypothesized membrane cleaning method that involves regulating the washing temperature. Therefore, the thermo-responsiveness of TRC was tested. The variations of the WCA of TRC, transmittance of TRC aqueous solution, and ZP and size of TRC in water, at different temperatures are plotted in Fig. 1c. As WCA is commonly used to represent the hydrophilicity/hydrophobicity of materials (Cui et al., 2019; Zhang et al., 2021), the upward trend of the WCA-temperature curve indicated that TRC became more hydrophobic at the elevated temperature. The original transparent (transmittance: ~90%) TRC aqueous solution (1 g/L) at 5 ^{o}C became opaque milky white with the increase of temperature, since the heightened hydrophobicity reduced the solubility. Specifically, the critical temperature point representing the switch for solution transparency, which is called the lower critical solution temperature (LCST) of thermo-responsive materials (Wang et al, 1998), was determined to be ~34 ^{o}C (SI, Fig. S9). The average size of TRC underwent a decline from ~4.78 nm at 5 ^{o}C to ~2.12 nm at 45 ^{o}C, and higher temperature gave rise to lower ZP. Chitosan backbones with protonated amino groups were positively charged (Lupa et al., 2022), whereas PNIPAM typically showed more negative ZP due to the adsorption of OH^- ions at higher temperatures when its structure collapsed (Utashiro et al., 2016). Hence, the downward ZP-temperature curve of TRC was attributed to the collapsed PNIPAM chains with more adsorbed OH^- ions which suppressed the positive charges of chitosan. The MD computation results in Fig. 1d displayed the temperature-dependent behaviour of the PNIPAM chain, which was similar to that of hydrophobic chains of protein in the folding process (Baldwin, 1986; Wolfenden et al., 2015): fewer intermolecular PNIPAM-water H-bonds (53, 34, and 20 at 5, 25, and 45 ^{o}C, respectively), but more intramolecular H-bonds within the PNIPAM chain (10, 17, and 22 at 5, 25, and 45 ^{o}C,

265 respectively), were formed at higher temperatures, engendering the collapsed chain. In
266 contrast, the chitosan chain did not change much at various temperatures (the SI, Fig.
267 S10). Potential link between the temperature-dependent bahaviour of the PNIPAM
268 chains of TRC to fouling control performance will be described later.
269
270 **3.2 Membrane fouling control performance**
271 **3.2.1 Effect of flocculant/coagulant type**
272 The rise in TMP, indicating membrane fouling development, for different FSUF
273 systems, with the single dosing of alum, PAM, and TRC, and the combined dosing of
274 alum and TRC (denoted as alum+TRC), over the 40 days of operation (3 membrane
275 cycles/stages), is illustrated in Fig. 2a. The TMP increased steadily during each stage
276 before S&S cleaning. Among the FSUF systems with the single dosing of
277 flocculant/coagulant, the TRC system displayed the slowest TMP growth rate; the TMP
278 at day 40 was 13.75 kPa in the TRC system, which was much less than the values (19.25
279 and 21.55 kPa, respectively) in the alum and PAM systems. When the TRC was
280 combined with alum, a further improvement in fouling development was achieved, with
281 the final TMP decreasing to 11.95 kPa. The S&S cleaning at the end of each stage was
282 effective in the removal of REV, with a substantial TMP decline; the remaining fouling
283 resistance corresponded to the IRR. Both REV and IRR in the different
284 flocculant/coagulant systems are depicted in Fig. 2b. The advantages of the alum+TRC
285 system over the other three systems in fouling mitigation were shown in the enhanced
286 reduction of both REV and IRR. As stated above in Section 2.2, the successive dosing
287 of alum and TRC can remove more potential fouling-causing materials prior to UF,
288 compared to the dosing of any single flocculant/coagulant (SI, Fig. S3). In addition,
289 another reason for the enhanced fouling reduction was attributed to the effective

membrane-surface-modification effect of residual TRC in the UF feed water, which was supported by both experimental and computational results (SI, Figs. S11-S12), specifically: When the UF membranes were used for direct filtration (without any pretreatment) of raw water (SI, Fig. S11), alum solution and TRC solution, the WCAs of used membranes were always lower than that of the pristine membrane, indicating that each of the hydrophilic materials originating from the raw water, alum, and TRC contributed to the hydrophilization of the UF membrane surface. Among them, TRC made the most contribution, with the lowest WCA value. Chemical computations demonstrated that the hydrophobic PNIPAM chain had a much larger BE with PVDF (the matrix material of the UF membrane) via hydrophobic association, than the chitosan backbone, other coagulant/flocculant, or any of the main contaminants in residual micro-flocs (the SI, Fig. S12). Hence, similar to the association of hydrophobic segments in proteins, PNIPAM chains of residual TRC and the hydrophobic PVDF chains on the UF membrane surface could be tightly bound, whereas the hydrophilic charged chitosan of TRC or other compositions of micro-flocs formed a water-exposed surface, which provided a protective hydration layer to inhibit accumulation of fouling material.

3.2.2 Effects of cleaning temperatures

The PNIPAM chains of TRC were found to be important in membrane surface modification in the alum+TRC system. As the hydrophobicity of the PNIPAM chains are temperature-dependent, the effects of both B&A and S&S cleaning temperature on the fouling control performance in the system were studied. The TMP development, as well as REV and IRR, are depicted in Figs. 2c-d, in which the FSUF system denoted by X ^{o}C/Y ^{o}C, referred to a cleaning mode with B&A cleaning at X ^{o}C and S&S cleaning

315 at Y ^{o}C.

316 The variations in the B&A cleaning temperature generated significant differences
317 in TMP growth from the first day(Fig. 2c). An elevated backwash water temperature
318 (X=45 ^{o}C) was beneficial for slowing down TMP growth, whereas the lower
319 temperature (X=5 ^{o}C) was detrimental with more severe fouling. The B&A cleaning
320 every 30 min gradually amplified the above differences in the following 39 days. At
321 day 40, the average TMP of the two systems with B&A cleaning temperatures of 5 ^{o}C
322 reached 15.75 kPa, while the average of the other two systems with B&A cleaning
323 temperatures of 45 ^{o}C was 6.08 kPa. Similar to the influence of B&A cleaning
324 temperature, a higher S&S cleaning water temperature promoted the decline of TMP;
325 however, the influence of the S&S cleaning temperature was less than that of the B&A
326 cleaning temperature. The 45 ^{o}C/45 ^{o}C cleaning mode in the FSUF system had the best
327 performance (Fig. 2c-d). Compared to the conventional cleaning process at room
328 temperature, the approach of moderately increasing the cleaning temperature in the
329 alum+TRC system substantially reduced the REV and IRR by 49.8%~61.3% and
330 73.9%~83.3%, respectively (Fig. 2d). However, in the FSUF system using alum alone
331 as the coagulant, the elevated temperature did not affect the TMP variation, REV and
332 IRR (the SI, Fig. S13). This implied that, although the increase of temperature will lead
333 to intensified activity of water molecules, the contribution of the intensified activity to
334 fouling mitigation was small. The significant fouling reduction at the elevated
335 temperature in the alum+TRC system was more likely attributable to the temperature-
336 responsiveness of TRC, which will be considered subsequently (in Section 3.3).

337 In addition to TMP, the surface morphology of the used membranes at day 40 was
338 examined using SEM and AFM, to show directly the membrane fouling. Before the
339 final S&S cleaning in stage 3, the membranes with cake layers on the surfaces were

observed using SEM. Images in Fig. 3a-f demonstrated that cake layers in the systems with B&A cleaning at both 25 ^{o}C (Fig. 3b) and 5 ^{o}C (Fig. 3e-f) covered nearly the whole membrane surface with a compact structure. In contrast, loose cake layers with obvious cracks were found in the two systems with elevated B&A cleaning temperature (Fig. 3c-d); between them, an elevated S&S cleaning temperature (in stages 1 and 2) also made the cake layers looser and thinner with larger cracks (Fig. 3c). The SEM observations implied that the raised cleaning temperature effectively damaged the cake layers, which was beneficial to lowering hydraulic resistance during the UF operation.

Subsequently, after cake layers were removed by S&S cleaning for the last time, the surfaces of the used membranes with only irreversible fouling were observed using AFM (Fig. 3g-l). Among AFM images, the system with the 45 ^{o}C/45 ^{o}C cleaning mode had the smallest surface roughness (R_q of 0.216; the closest to the value of a pristine membrane), indicating the effectiveness of elevated cleaning temperature in the mitigation of irreversible fouling. Taking the R_q value of the 25 ^{o}C/25 ^{o}C mode as the reference, irrespective of the S&S cleaning temperature, the membrane surfaces in the two systems with a B&A cleaning temperature of 45 ^{o}C had a smaller R_q, whereas those in the other two systems with a B&A cleaning of 5 ^{o}C had a larger R_q. Such a result confirmed the dominant influence of the B&A cleaning temperature over the S&S cleaning temperature on irreversible fouling control.

3.3 Mechanisms for the membrane cleaning approach based on temperature regulation

The above results confirmed the effectiveness of increasing cleaning temperature for fouling control in the FSUF system with the dosing of TRC. To reveal the mechanisms, an in-depth investigation involving statistical analyses, instrumental

365 characterizations, and chemical computations, was carried out as follows.

366 **3.3.1 Impact on the accumulation of contaminants on the membranes**

367 The flows of the principal materials in solution, involving inorganic (ISS) and
368 organic (total organic carbon (TOC)) substances,) total phosphorous (TP), TRC and
369 alum, which might impact membrane fouling, in the FSUF process, were visualized
370 using Sankey diagrams (as shown in Fig. 4a and the SI, Fig. S14); these diagrams have
371 been widely employed for performing the path analytics and understanding the potential
372 links of complex data (Graedel, 2019; Van Vuuren et al., 2019). Control tests, using raw
373 water without spiked antibiotics as a reference, demonstrated that the influence of
374 antibiotics on fouling could be neglected (see details in the SI, Fig. S15), since the
375 concentrations of spiked antibiotics were 4 log-units lower than the above-mentioned
376 principal materials in water. Hence, antibiotic flows were not analyzed here. As
377 illustrated in Fig. 4a, and the SI, Fig. S14, material flows in the flocculation and
378 sedimentation units were the same in the FSUF systems with different cleaning modes,
379 as the same FS operation parameters were used. After sedimentation, the residual
380 materials in the UF feed water were divided into three parts, involving those in the
381 fouling material on the membrane, in the sludge at the UF tank bottom, and in the final
382 produced water. As materials adhering to the membranes directly influence their
383 permeability, PCA and correlation analysis of the final TMP value and different
384 percentages of materials on the membranes were performed as depicted in Fig. 4b-c.

385 According to PCA-loading plots (Fig. 4b), only one statistically significant
386 principal component (PC1) was found, explaining 96.99% of the total variance (a
387 considerably high value to show the accurate description of the real experimental data
388 by the PCA model). With respect to PC1, different variables were grouped into two
389 species – the positive-value (TMP, and percentages of alum, ISS, TP and TOC on the

membrane) and the negative-value species (percentage of TRC). It could be inferred that TRC left on the membrane inhibited the accumulation of ISS, TOC and TP and the increase of TMP. The linear correlation between TMP and other variables in Fig. 4c provided quantitative data describing the relationships. ISS, TOC and TP on the membranes, which could generate inorganic, organic and bio fouling (Gao et al., 2011; Li et al., 2023), respectively, were positively correlated with TMP with large regression coefficients (R^2). The amounts of ISS,TOC, or TP accumulated on the final membrane in the 45 ^{o}C/45 ^{o}C system was the lowest among the five systems, indicating that the increased cleaning temperature effectively alleviated accumulation of these contaminants. This further weakened the mass transfer of small-sized contaminants (those smaller than 20 nm in the effluent after FS, as shown in the SI, Fig. S16) from the membrane surface to the pores. As depicted in the pore size distribution curves of the used membranes after the final S&S cleaning (Fig. 4d), although peaks and the average pore sizes shifted towards smaller values after use due to the blockage of pores, those in the 45 ^{o}C/45 ^{o}C system were the closest to the corresponding values of the pristine membrane.

3.3.2 Impact on the surface-modification of UF

Regarding the impact of externally dosed coagulant and flocculant on the UF membrane, the results in Fig. 4c showed that alum and TRC had opposite influences on TMP. The amount of alum on the membrane was positively (slope>0) correlated (R^2=0.781) with TMP, implying that the residual coagulant on the membrane aggravated inorganic fouling (Ma et al., 2014). However, the inverse correlation (slope<0) between TMP and TRC left on the membrane was found to be more significant (R^2=0.984). This indicated that the hydrophobic modified flocculant

deposited on the membrane did not intensify organic fouling, but was conducive to fouling reduction Among the five systems, the largest amount of TRC but lowest amount of alum left on the membranes appeared in the 45 ^{o}C/45 ^{o}C system (Fig. 4c), giving rise to the lowest TMP at the end of the FSUF operation. In the same system, the most significant surface-modification-effect with the lowest WCA value of the used membrane (Fig. 4e) was found. Hence, similar to the strengthened hydrophobic association of hydrophobic chains in proteins at elevated temperatures (Baldwin, 1986; Wolfenden et al., 2015), the increase of cleaning temperature strengthens the membrane-surface-modification role of TRC.

Direct evidence to support this was provided by the computed BEs of different fragments adsorbed onto the PVDF interface in water at different temperatures, as illustrated in Fig. 5.The fragments of TRC (chitosan and PNIPAM chains), NOM and ISS (using kaolin as a representative) were computed. According to Fig. 5, at any temperature, the BE of the PNIPAM-PVDF complexes formed by hydrophobic association were notably greater than those of other complexes, confirming that the surface-modification effect of TRC was unlikely to be significantly affected by the coexistence of other contaminants. For the PNIPAM-PVDF complexes (Fig. 5a-c), the rise of temperature remarkably enhanced the hydrophobic association, with BE values from 15.25 kcal/mol at 5 ^{o}C to 40.56 kcal/mol at 45 ^{o}C. This was consistent with previous findings in protein folding that hydrophobic association was an entropy-increase-driven process (Eisenberg and Sawaya, 2016), for which the elevated temperature was favored according to thermodynamic relationships. Consequently, the membrane-surface-modification effect of TRC was strengthened by both the B&A and SS cleaning at an elevated temperature.

3.3.3 Impact on the structure of fouling on the membrane

As well as inhibiting contaminant accumulation and strengthening the surface-modification effect of TRC, the increased cleaning temperature can affect the structure of fouling on the membrane, which may be similar to the impact of temperature on the protein structure. Building materials of the fouling deposits, involving the coagulant, the flocculant, ISS, NOM and so on, were the same to those of flocs generated in the same FSUF system. Thus, the influence of temperature on fouling structure was qualitatively similar to that on the floc structure, of which the in-situ characterizations have been well established (Yang et al., 2013). The real-time variations of floc size and fractal dimension (D_F) at different temperatures and velocity gradients (G values) were monitored and are shown in Fig. 6a-b. In the tests, prior to changing the water temperature (the starting point, t=0 min), flocs were fully grown under a rapid mix at G= 128 s^{-1} for 5 min, and a subsequent flocculation at G= 16 s^{-1} for 15 min at 25 ^{o}C. Subsequently, three stages of experiments at different temperatures were successively designed and conducted, involving stage 1 at the unchanged G value (16 s^{-1}), stage 2 for floc breakage at G= 128 s^{-1}, and stage 3 for floc regrowth at G= 16 s^{-1}). A floc strength factor (F_1) and regrowth factor (F_2) under different conditions, were calculated:

$$F_1=d_2/d_1 \quad \text{(Eq.3)}$$

$$F_2=(d_3-d_2)/(d_1-d_2) \quad \text{(Eq.4)}$$

where d_1, d_2, and d_3 were the floc sizes at the end of stages 1, 2, and 3, respectively. As depicted in Fig. 6a-b, in stage 1, although the G value was kept unchanged, the higher temperature induced the flocs to became slightly smaller and less compact (D_F decline) spontaneously. This implied that the increased temperature weakened floc stability. Such an effect was enhanced at a greater G value in stage 2: flocs at 45 ^{o}C, with a lower F_1 value, were much more easily broken than flocs at the other two temperatures.

Therefore, it could be inferred, through a reasonable analogy, that fouling material with a destabilized structure at the elevated temperature was more easily degraded and removed from the membrane under turbulent conditions caused by cleaning. Furthermore, the results in stage 3 demonstrated that the regrowth capacity of the broken flocs at 45 ^{o}C was the worst (substantial decline of F_2 value). In other words, the increased temperature caused more severe irreversible damage to the structure of flocs, as well as to that of the fouling material, analogously. The collapsed TRC structure at the elevated temperature causes the fouling material to become unstable and thus be removed more easily. The temperature-induced structural damage was also related to the thermo-responsiveness of PNIPAM chains, according to the computed BEs of PNIPAM-NOM and PNIPAM-ISS complexes (Fig. 6c-h): With the rise of temperature, the BEs, representing the stability, of both complexes decreased; since TRC, NOM and ISS were the main building materials of fouling (Ho et al., 2022), the fouling structure was thus weakened.

3.4 Evaluation of other measures of performance: water purification, membrane stability, and economic aspects

Other important measures of performance of the FSUF process, involving water purification, membrane stability, and economic aspects, which might be influenced by the elevated cleaning temperature, were evaluated as follows.

3.4.1 Water purification

Water quality improvement is a priority goal of water treatment, and it was important to establish whether the elevated cleaning temperature would affect the produced water quality. The quality of the produced water by the different FSUF systems is summarized in the SI, Figs. S6 and S17. The dosing of TRC in the FSUF

process remarkably improved the REs of the antibiotics (SI, Fig. S15), due to the enhanced hydrophobic association between the hydrophobic-modified flocculant and antibiotics, as previously reported (Wang et al., 2022). For the alum+TRC system which had the highest REs of the antibiotics (SI, Fig. S17), changing the cleaning temperature in the UF tank did not lead to significant differences in water quality (SI, Fig. S6). This was attributed to the fact that the major contribution to contaminant removal occurred in the FS stage. Despite this, compared to other cleaning modes, the minor improvement, rather than a deterioration, of REs of contaminants in the 45 ^{o}C/45 ^{o}C system (SI, Fig. S18) eliminated any concerns about adverse water quality impacts by the elevating-temperature cleaning approach. The minor improvement of REs was ascribed to the improved cleaning performance at the higher temperature which inhibited penetration (mass transfer) of contaminants through the membrane, as aforementioned.

In addition to the contaminants in the produced water, attention was also given to the presence of residual TRC and Al^{3+}, considering the potential risks associated with the flocculant and the coagulant. For TRC, both the natural chitosan backbones and the PNIPAM chains (widely used for in-vivo drug delivery) of TRC are environmentally-benign and biocompatible polymers (Sun et al., 2014). In addition, according to the test results (Fig. 4a), TRC was not detected in the final produced water, since the size of TRC (Fig. 1c) was much larger than the UF membrane pores. With respect to residual Al ions, according to the Sankey diagram in Fig. 4a, the Al concentration in the produced water was 0.027 mg/L, which is much lower than the upper limit (0.2 mg/L) in Chinese national standards for drinking water quality (GB 5749-2022). Therefore, it was concluded that the successive dosing of TRC and alum in the FSUF system did not pose significant, direct risks to the produced water quality.

3.4.2 Membrane stability

PVDF is well-known for its high chemical stability with heat resistance (Liu et al., 2011). Despite this, the physical stability of the membranes under the conditions of repeated temperature changes was uncertain. The stress-strain curves of the pristine membrane, and used membranes (after the final S&S cleaning), for the different FSUF systems are shown in the SI (Fig. S19), which indicated a negligible difference in behavior among all the membranes. This result demonstrated that the elevated cleaning water temperature did not appear to affect the mechanical integrity of the UF membranes. On the other hand, as previously mentioned in Section 3.3.1, although membrane pores were blocked to various degrees after use in all FSUF systems (Fig. 4d), the degree of pore blockage in the 45 ^{o}C/45 ^{o}C system was the lowest. Thus, compared to the conventionally operated 25 ^{o}C/25 ^{o}C mode, the elevated cleaning temperature slightly improved the pore structure stability of the membrane.

3.4.3 Economic analysis

A preliminary analysis of the economic feasibility of applying an elevated-cleaning-temperature approach was explored, in view of the additional cost of energy for heating the cleaning water for the B&A and S&S (C_{HE}) operations. By assuming the use of industrial low-grade waste heat (e.g. industrial cooling water at 90 ^{o}C) (Adhikary et al., 2020; Zhou et al., 2015) for heating the cleaning water at an initial temperature of 25 ^{o}C in large-scale applications as a basis, the C_{HE} was calculated:

$$C_{HE}=PPU_{cw}\times(m_{BA}+m_{SS})\times(T_{cleaning}-T_{initial})/((T_{cw}-T_{cleaning})\times\varepsilon) \quad \text{(Eq. 5)}$$

where: PPU_{cw} (CNY/kg) is the price per unit of industrial cooling water at 90 ^{o}C; m_{BA} (kg) and m_{SS} (kg) are the total massmass of water used for B&A and S&S cleaning, respectively; $T_{cleaning}$ (^{o}C), $T_{initial}$ (^{o}C), and T_{cw} (^{o}C) are the temperatures of backwash or

soaking water (45 ^{o}C), initial water (25 ^{o}C), and the used industrial cooling water (90 ^{o}C), respectively; ε is the heat exchange efficiency.

Based on the values as given in the SI (Table S2), the C_{HE} for the 40 days of FSUF operation (480 L of treated water in total) was ~0.097 Chinese Yuan (CNY). That is to say, the cost was ~0.202 CNY (~US$ 0.029)/(m^3 of water) for the elevated-cleaning-temperature approach to significantly alleviate membrane fouling (the reductions of REV and IRR were 49.8%~61.3% and 73.9%~83.3%, respectively, as mentioned above). As well as the very low energy cost, the mitigated fouling during the UF operation could save, (i) pumping energy costs (one of the major operational expenses) due to fouling (Jafari et al., 2021; Porcelli and Judd, 2010), (ii) membrane replacement costs (another of the major operational expenses) when the membrane service lifetime is reached after extensive fouling formation (Jafari et al., 2021; Porcelli and Judd, 2010), and (iii) chemicals (such as acids and bases) in conventional membrane cleaning. Considering these aspects, it could be regarded as potentially economically feasible to apply the proposed cleaning approach by raising the cleaning water temperature to mitigate fouling.

4. Conclusions

The hydrophobic-modified flocculant TRC was found to have temperature-dependent hydrophobicity, which was similar to the characteristics of natural proteins. Inspired by the protein folding phenomenon, the approach of using membrane cleaning temperature as the trigger to induce deposited, residual TRC after FS to reduce subsequent UF fouling was proposed and verified in this work. The alum+TRC FSUF system was found to have notable advantages in fouling control over the conventional alum system. A moderately elevated cleaning water temperature (45 ^{o}C), applied in both

B&A and S&S cleaning in the alum+TRC system, gave rise to substantial reductions in REV and IRR of 49.8%~61.3% and 73.9%~83.3%, respectively, of which the elevated temperature of B&A cleaning contributed the major part. The mechanisms for the enhanced fouling mitigation performance of the novel approach were: (i) inhibited contaminant accumulation onto membranes, (ii) the strengthened membrane-surface-modification effect of TRC, and (iii) the weakened structure of the foulant layer at the elevated cleaning temperature. Other key measures of performance, involving water purification, membrane stability and economic aspects, also confirmed the advantages and feasibility of the novel approach. In summary, this work has demonstrated more beneficial role of hydrophobic-modified flocculants in the treatment of surface water by a flocculation-sedimentation-ultrafiltration process.

Acknowledgments

The financial support from the Natural Science Foundation of China (51978341), the Special Foundation for the Development of Science and Technology of Xinjiang Bingtuan of China (2022DB025), the Industry-University Collaborative Education Project of MOE of China (220602905023838), and the Jiangsu Collaborative Innovation Center of Biomedical Functional Materials, are gratefully acknowledged. The authors would also like to thank Ms. Ying Zhu and the Scientific Computing Center of NNU for the helpful support for computational simulations in this work.

References

Adhikary, S., Islam, M.S., Touati, K., Sultana, S., Ramamurthy, A.S., Rahaman, M.S., 2020. Increased power density with low salt flux using organic draw solutions for pressure-retarded osmosis at elevated temperatures. Desalination 484,

114420

Baldwin, R.L., 1986. Temperature dependence of the hydrophobic interaction in protein folding. Proc. Natl. Acad. Sci. USA 83(21), 8069-8072.

Chen, Q., Zheng, J.W., Yang, Q., Dang, Z., Zhang, L.J., 2019. Effect of carbon chain structure on the phthalic acid esters (PAEs) adsorption mechanism by mesoporous cellulose biochar. Chem. Eng. J. 362, 383-391.

Colvin, M.T., Silvers, R., Ni, Q.Z., Can, T.V., Sergeyev, I., Rosay, M., Donovan, K.J., Michael, B., Wall, J., Linse, S., Griffin, R.G., 2016. Atomic resolution structure of monomorphic a beta(42) amyloid fibrils. J. Am. Chem. Soc. 138(30), 9663-9674.

Cui, C., Fan, C., Wu, Y., Xiao, M., Wu, T., Zhang, D., Chen, X., Liu, B., Xu, Z., Qu, B., Liu, W., 2019. Water-triggered hyperbranched polymer universal adhesives: From strong underwater adhesion to rapid sealing hemostasis. Adv. Mater. 31(49), 1905761.

Demissie, H., Lu, S., Jiao, R., Liu, L., Xiang, Y., Ritigala, T., Ajibade, F.O., Mihiranga, H.K.M., An, G., Wang, D., 2021. Advances in micro interfacial phenomena of adsorptive micellar flocculation: Principles and application for water treatment. Water Res. 202, 117414.

Dill, K.A., Ozkan, S.B., Shell, M.S., Weikl, T.R., 2008. The protein folding problem. Annu. Rev. Biophys. 37, 289-316.

Eisenberg, D.S., Sawaya, M.R., 2016. Implications for Alzheimer's disease of an atomic resolution structure of amyloid-beta(1-42) fibrils. Proc. Natl. Acad. Sci. USA 113(34), 9398-9400.

Gan, Y.H., Zhang, L., Zhang, S.J., 2021. The suitability of titanium salts in coagulation removal of micropollutants and in alleviation of membrane fouling. Water Res.

205, 117692.

Gao, W., Liang, H., Ma, J., Han, M., Chen, Z.L., Han, Z.S., Li, G.B., 2011. Membrane fouling control in ultrafiltration technology for drinking water production: A review. Desalination 272(1-3), 1-8.

Graedel, T.E., 2019. Material flow analysis from origin to evolution. Environ. Sci. & Technol. 53(21), 12188-12196.

Guo, Y., Liang, H., Li, G., Xu, D., Yan, Z., Chen, R., Zhao, J., Tang, X., 2021. A solar photo-thermochemical hybrid system using peroxydisulfate for organic matters removal and improving ultrafiltration membrane performance in surface water treatment. Water Res. 188, 116482.

He, H.Y., Qiu, W., Liu, Y.L., Yu, H.R., Wang, L., Ma, J., 2021. Effect of ferrate pre-oxidation on algae-laden water ultrafiltration: Attenuating membrane fouling and decreasing formation potential of disinfection byproducts. Water Res. 190, 116690.

Ho, Q.N., Fettweis, M., Spencer, K.L., Lee, B.J., 2022. Flocculation with heterogeneous composition in water environments: A review. Water Res. 213, 118147.

Jafari, M., Vanoppen, M., van Agtmaal, J.M.C., Cornelissen, E.R., Vrouwenvelder, J.S., Verliefde, A., van Loosdrecht, M.C.M., Picioreanu, C., 2021. Cost of fouling in full-scale reverse osmosis and nanofiltration installations in the Netherlands. Desalination 500, 114865.

Larsen, T.A., Hoffmann, S., Luthi, C., Truffer, B., Maurer, M., 2016. Emerging solutions to the water challenges of an urbanizing world. Science 352(6288), 928-933.

Li, B.D., Ma, J., Qiu, W., Li, W.Q., Zhang, B., Ding, A., He, X., 2022. In-situ utilization

of membrane foulants (FeO_x+MnO_x) for the efficient membrane cleaning. Water Res. 210, 118004.

Li, Q.L., Elimelech, M., 2004. Organic fouling and chemical cleaning of nanofiltration membranes: Measurements and mechanisms. Environ. Sci. Technol. 38(17), 4683-4693.

Li, Y.Y., Wang, Y.D., Jin, J., Tian, Z.Q., Yang, W.B., Graham, N.J.D., Yang, Z., 2023, Enhanced removal of trace pesticides and alleviation of membrane fouling using hydrophobic-modified inorganic-organic hybrid flocculants in the flocculation-sedimentation-ultrafiltration process for surface water treatment. Water Res. 229, 119447.

Liu, F., Hashim, N.A., Liu, Y.T., Abed, M.R.M., Li, K., 2011. Progress in the production and modification of PVDF membranes. J. Membr. Sci. 375(1-2), 1-27.

Liu, J., Cheng, S., Cao, N., Geng, C., He, C., Shi, Q., Xu, C., Ni, J., DuChanois, R.M., Elimelech, M., Zhao, H., 2019. Actinia-like multifunctional nanocoagulant for single-step removal of water contaminants. Nat. Nanotechnol. 14(1), 64-71.

Liu, T., Lian, Y., Graham, N., Yu, W., Rooney, D., Sun, K., 2017. Application of polyacrylamide flocculation with and without alum coagulation for mitigating ultrafiltration membrane fouling: Role of floc structure and bacterial activity. Chem. Eng. J. 307, 41-48.

Long, Y., Yu, G.Y., Dong, L., Xu, Y.C., Lin, H.J., Deng, Y., You, X.J., Yang, L.N., Liao, B.Q., 2021. Synergistic fouling behaviors and mechanisms of calcium ions and polyaluminum chloride associated with alginate solution in coagulation-ultrafiltration (UF) process. Water Res. 189, 116665.

Lupa, D., Plazinski, W., Michna, A., Wasilewska, M., Pomastowski, P., Golebiowski, A., Buszewski, B., Adamczyk, Z., 2022. Chitosan characteristics in electrolyte

665 solutions: Combined molecular dynamics modeling and slender body
666 hydrodynamics. Carbohydr. Polym. 292, 119676.
667 Ma, B.W., Yu, W.Z., Liu, H.J., Qu, J.H., 2014. Effect of low dosage of coagulant on the
668 ultrafiltration membrane performance in feedwater treatment. Water Res. 51,
669 277-283.
670 Melo-Guimaraes, A., Torner-Morales, F.J., Duran-Alvarez, J.C., Jimenez-Cisneros,
671 B.E., 2013. Removal and fate of emerging contaminants combining biological,
672 flocculation and membrane treatments. Water Sci. Technol. 67(4), 877-885.
673 Porcelli, N., Judd, S., 2010. Chemical cleaning of potable water membranes: The cost
674 benefit of optimisation. Water Res. 44(5), 1389-1398.
675 Su, Z., Liu, T., Li, X., Graham, N., Yu, W., 2021. Beneficial impacts of natural
676 biopolymers during surface water purification by membrane nanofiltration.
677 Water Res. 201, 117330.
678 Sun, T.M., Zhang, Y.S., Pang, B., Hyun, D.C., Yang, M.X., Xia, Y.N., 2014. Engineered
679 nanoparticles for drug delivery in cancer therapy. Angew. Chemie. Int. Ed.
680 53(46), 12320-12364.
681 Utashiro, Y., Takiguchi, M., Satoh, M., 2016. Zeta potential of PNIPAM microgel
682 particles dispersed in water-effects of charged radical initiators vs. OH^- ion
683 adsorption. Colloid Polym. Sci. 295, 45-52.
684 Van Vuuren, D.P., Bijl, D.L., Bogaart, P., Stehfest, E., Biemans, H., Dekker, S.C.,
685 Doelman, J.C., Gernaat, D.E.H.J., Harmsen, M., 2019. Integrated scenarios to
686 support analysis of the food-energy-water nexus. Nat. Sustain. 2(12), 1132-1141.
687 Walti, M.A., Ravotti, F., Arai, H., Glabe, C.G., Wall, J.S., Bockmann, A., Guntert, P.,
688 Meier, B.H., Riek, R., 2016. Atomic-resolution structure of a disease-relevant A
689 beta(1-42) amyloid fibril. Proc. Natl. Acad. Sci. USA 113(34), 4976-4984.

690 Wang, X., Qiu, X., Wu, C., 1998. Comparison of the coil-to-globule and the globule-
691 to-coil transitions of a single poly(N-isopropylacrylamide) homopolymer chain
692 in water. Macromolecules 31(9), 2972-2976.
693 Wang, Z.Z., Li, Y.Y., Hu, M., Lei, T., Tian, Z.Q., Yang, W.B., Yang, Z., Graham, N.J.D.,
694 2022. Influence of DOM characteristics on the flocculation removal of trace
695 pharmaceuticals in surface water by the successive dosing of alum and
696 moderately hydrophobic chitosan. Water Res. 213, 118163.
697 Wilkinson, J., Hooda, P.S., Barker, J., Barton, S., Swinden, J., 2017. Occurrence, fate
698 and transformation of emerging contaminants in water: An overarching review
699 of the field. Environ. Pollut. 231, 954-970.
700 Wolfenden, R., Lewis, C.A., Yuan, Y., Carter, C.W., 2015. Temperature dependence of
701 amino acid hydrophobicities. Proc. Natl. Acad. Sci. USA 112(24), 7484-7488.
702 Xu, L., Zhou, Z., Graham, N.J.D., Liu, M.J., Yu, W.Z., 2021. Enhancing ultrafiltration
703 performance by gravity-driven up-flow slow biofilter pre-treatment to remove
704 natural organic matters and biopolymer foulants. Water Res. 195, 117010.
705 Yang, B.X., Wen, Q.X., Chen, Z.Q., Tang, Y.C., 2022. Potassium ferrate combined with
706 ultrafiltration for treating secondary effluent: Efficient removal of antibiotic
707 resistance genes and membrane fouling alleviation. Water Res. 217, 118374.
708 Yang, Z., Hou, T., Ma, J., Yuan, B., Tian, Z., Yang, W., Graham, N.J.D., 2020. Role of
709 moderately hydrophobic chitosan flocculants in the removal of trace antibiotics
710 from water and membrane fouling control. Water Res. 177, 115775.
711 Yang, Z., Yang, H., Jiang, Z.W., Huang, X., Li, H.B., Li, A.M., Cheng, R.S., 2013. A
712 new method for calculation of flocculation kinetics combining Smoluchowski
713 model with fractal theory. Colloids Surf. A Physicochem. Eng. Asp. 423, 11-19.
714 Yang, Z., Zhao, L.N., Hu, M., Cai, D., Tian, Z.Q., Baeyens, J., Dewil, R., Qin, P.Y.,

715 Yang, W.B., Graham, N.J.D., 2021. Hydrophobic-modified metal-hydroxide
716 nanoflocculants enable one-step removal of multi-contaminants for drinking
717 water production. iScience 24(5), 102491.
718 Zhou, X.S., Gingerich, D.B., Mauter, M.S., 2015. Water treatment capacity of forward-
719 osmosis systems utilizing power-plant waste heat. Ind. Eng. Chem. Res. 54(24),
720 6378-6389.
721 Zhang, J., Jia, K., Huang, Y., Liu, X., Xu, Q., Wang, W., Zhang, R., Liu, B., Zheng, L.,
722 Chen, H., Gao, P., Meng, S., Lin, L., Peng, H., Liu, Z. 2021. Intrinsic wettability
723 in pristine graphene. Advanced Materials 34(6), 2103620.

Captions

Table 1. Water quality parameters of the untreated raw water.

Fig. 1. (a) Chemical structure of TRC; (b) Schematic diagram of the continuous-flow FSUF apparatus; (c) Variation in water contact angle (WCA) of TRC, transmittance (T) of TRC solution, average size and zeta potential (ZP) of TRC in aqueous solutions with temperature; (d) Optimized structures of TRC in water phase (TRC and water molecules are separated in the images to better illustrate the intermolecular H-bonds; the numbers of intermolecular H-bonds between TRC and water, and intramolecular H-bonds in TRC, are marked) at different temperatures.

Fig. 2. (a and c) TMP growth with time, and (b and d) reversible and irreversible membrane resistances, in different FSUF systems with (a and b) different flocculants and/or coagulant, and (c and d) alum+TRC using different cleaning temperatures (X ^{o}C/Y ^{o}C refers to a cleaning mode with B&A cleaning at X ^{o}C and S&S cleaning at Y ^{o}C).

Fig. 3. (a-f) SEM images of membranes with cake layers on the surfaces, and (g-l) AFM images of membranes with cake layer removed from the surfaces at day 40, in FSUF systems with alum+TRC using different cleaning temperatures (X ^{o}C/Y ^{o}C refers to a cleaning mode with B&A cleaning at X ^{o}C and S&S cleaning at Y ^{o}C).

Fig. 4. (a) Material flow in the FSUF system with alum+TRC using the cleaning temperature mode of 45 ^{o}C/45 ^{o}C; (b) Principal component analysis among the final TMP and percentages of different materials on the membranes; (c) Linear correlation of the final TMP with percentages of different materials on the membranes in different FSUF systems (full: 5 ^{o}C/5 ^{o}C; empty: 5 ^{o}C/45 ^{o}C; upper half: 25 ^{o}C/25 ^{o}C; lower half: 45 ^{o}C/5 ^{o}C; cross: 45 ^{o}C/45 ^{o}C); (d) Pore size distributions and (e) water contact angles, of pristine and used membranes.

Fig. 5. Optimized structures and corresponding binding energies of different complexes formed between PVDF and various components (a-c: chitosan backbone; d-f: PNIPAM chain; g-i: representative NOM fragment; j-l: representative ISS fragment) in water at (a, d, g, and j) 5 ^{o}C, (b, e, h, and k) 25 ^{o}C, and (c, f, i, and l) 45 ^{o}C.

Fig. 6. (a and b) Real-time variations of (a) floc size and (b) D_F at different temperatures and velocity gradients; (c-h) Optimized structures and corresponding binding energies of different complexes formed between PNIPAM chain and various components ((c-e) representative NOM fragment; (f-h) representative ISS fragment) at (c and f) 5 ^{o}C, (d and g) 25 ^{o}C, and (e and h) 45 ^{o}C.

Click here to access/download;Table (Editable version);Table 1R.docx

Table 1. Water quality parameters of the untreated raw water.

pH	Turbidity (NTU)	ISS[a] (mg/L)	DOC (mg/L)	UV_{254} (cm^{-1})	SUVA (L/(mg·m))	TP (mg P/L)	Concentration of each antibiotic (μg/L)	Concentration of Al^{3+} (mg/L)
7.53	14.2	13.5	6.59	0.16	2.40	0.116	0.10	0.0012

[a] Inorganic suspended solids

Figure 1

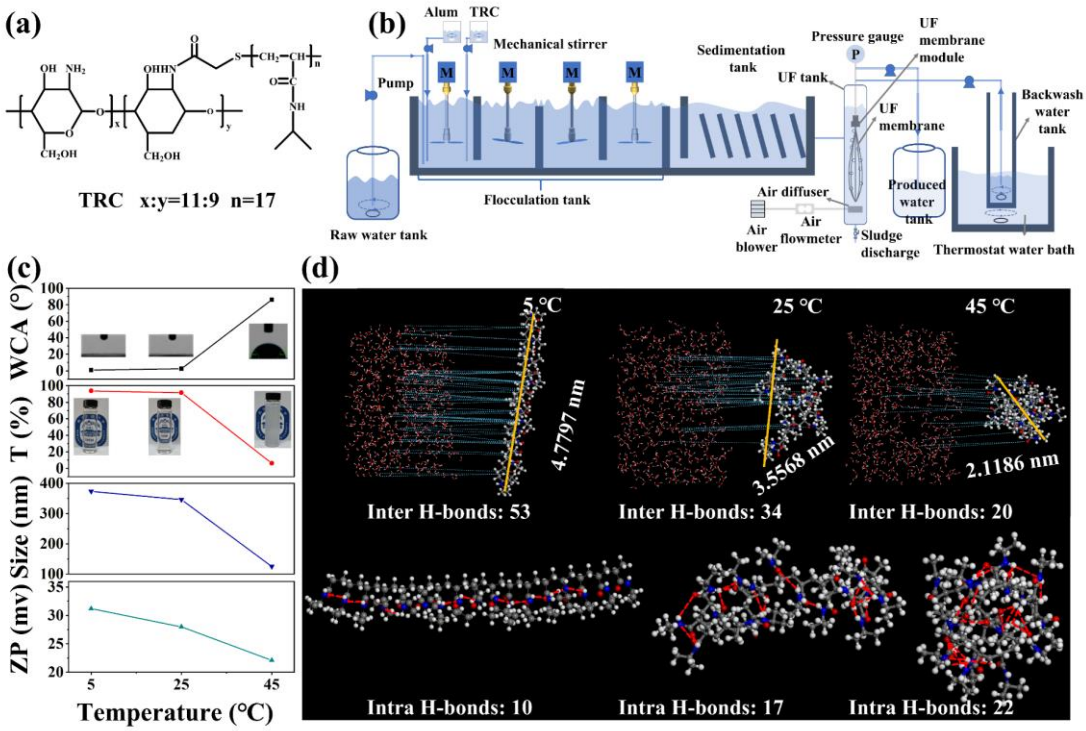


Fig. 1. (a) Chemical structure of TRC; (b) Schematic diagram of the continuous-flow FSUF apparatus; (c) Variation in water contact angle (WCA) of TRC, transmittance (T) of TRC solution, average size and zeta potential (ZP) of TRC in aqueous solutions with temperature; (d) Optimized structures of TRC in water phase (TRC and water molecules are separated in the images to better illustrate the intermolecular H-bonds; the numbers of intermolecular H-bonds between TRC and water, and intramolecular H-bonds in TRC, are marked) at different temperatures.

Figure 2

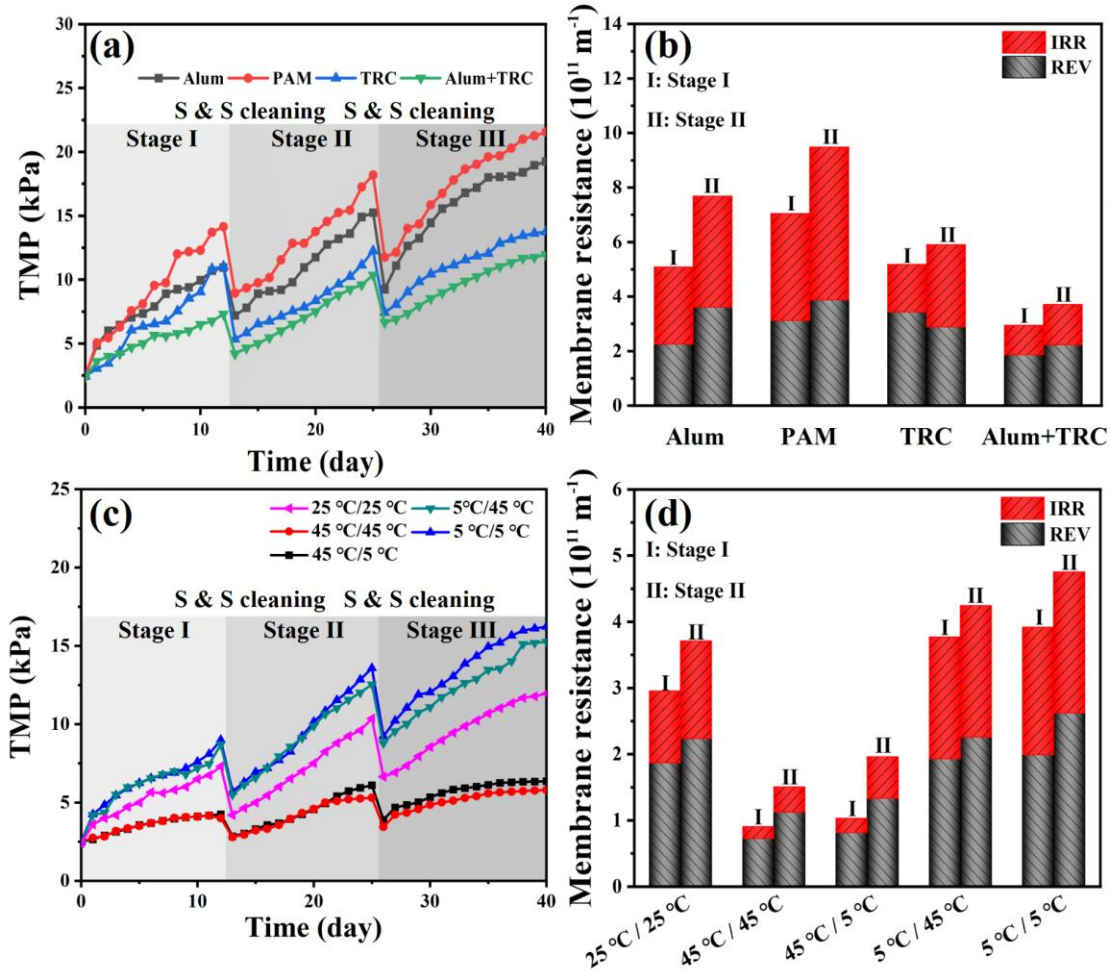


Fig. 2. (a and c) TMP growth with time, and (b and d) reversible and irreversible membrane resistances, in different FSUF systems with (a and b) different flocculants and/or coagulant, and (c and d) alum+TRC using different cleaning temperatures (X ^{o}C/Y ^{o}C refers to a cleaning mode with B&A cleaning at X ^{o}C and S&S cleaning at Y ^{o}C).

Figure 3

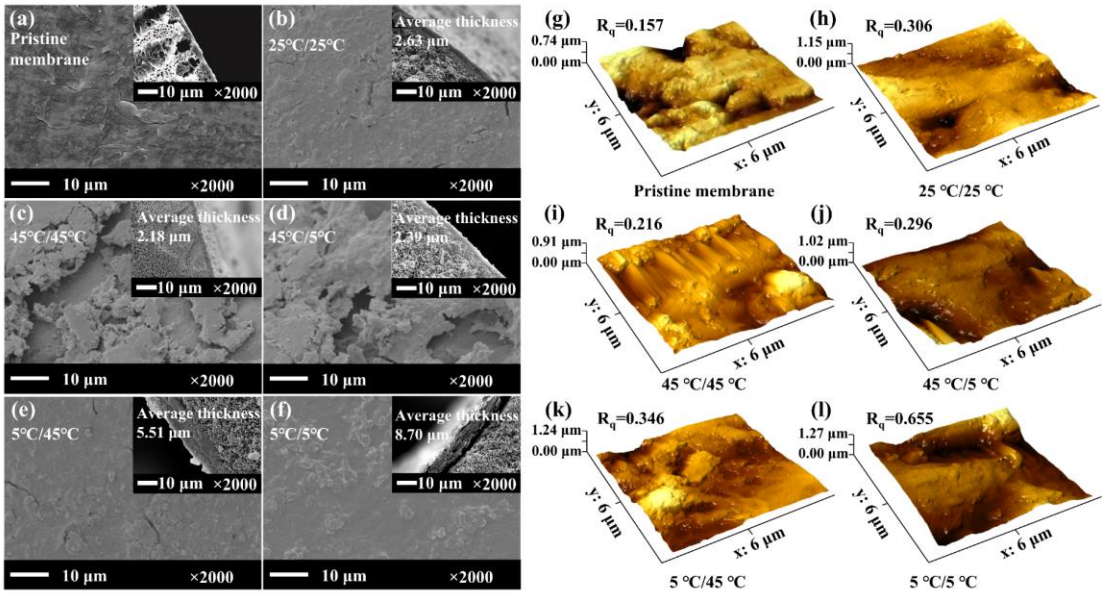


Fig. 3. (a-f) SEM images of membranes with cake layers on the surfaces, and (g-l) AFM images of membranes with cake layer removed from the surfaces at day 40, in FSUF systems with alum+TRC using different cleaning temperatures (X ^{o}C/Y ^{o}C refers to a cleaning mode with B&A cleaning at X ^{o}C and S&S cleaning at Y ^{o}C).

Figure 4

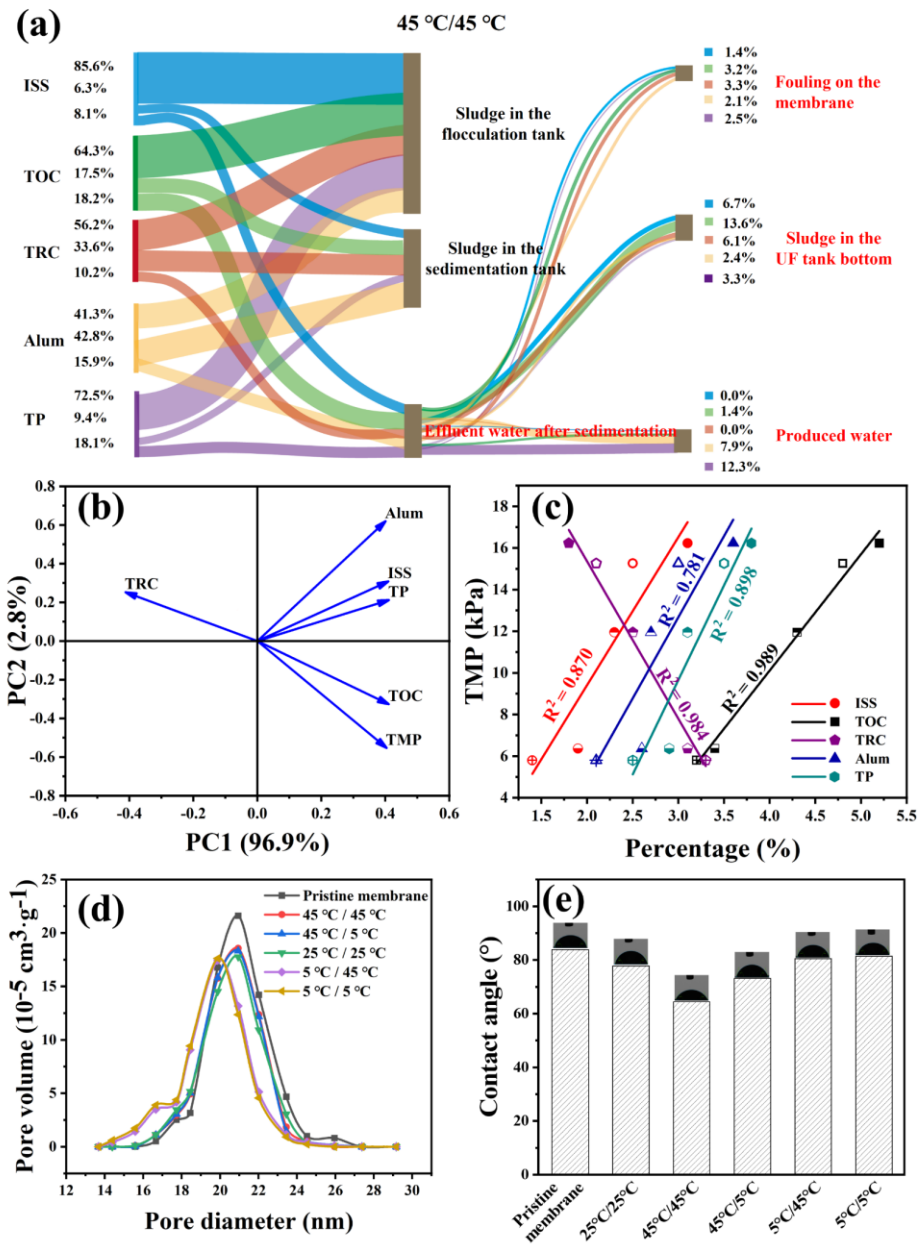


Fig. 4. (a) Material flow in the FSUF system with alum+TRC using the cleaning temperature mode of 45 °C/45 °C; (b) Principal component analysis among the final TMP and percentages of different materials on the membranes; (c) Linear correlation of the final TMP with percentages of different materials on the membranes in different FSUF systems (full: 5 °C/5 °C; empty: 5 °C/45 °C; upper half: 25 °C/25 °C; lower half: 45 °C/5 °C; cross: 45 °C/45 °C); (d) Pore size distributions, and (e) water contact angles, of pristine and used membranes.

Figure 5

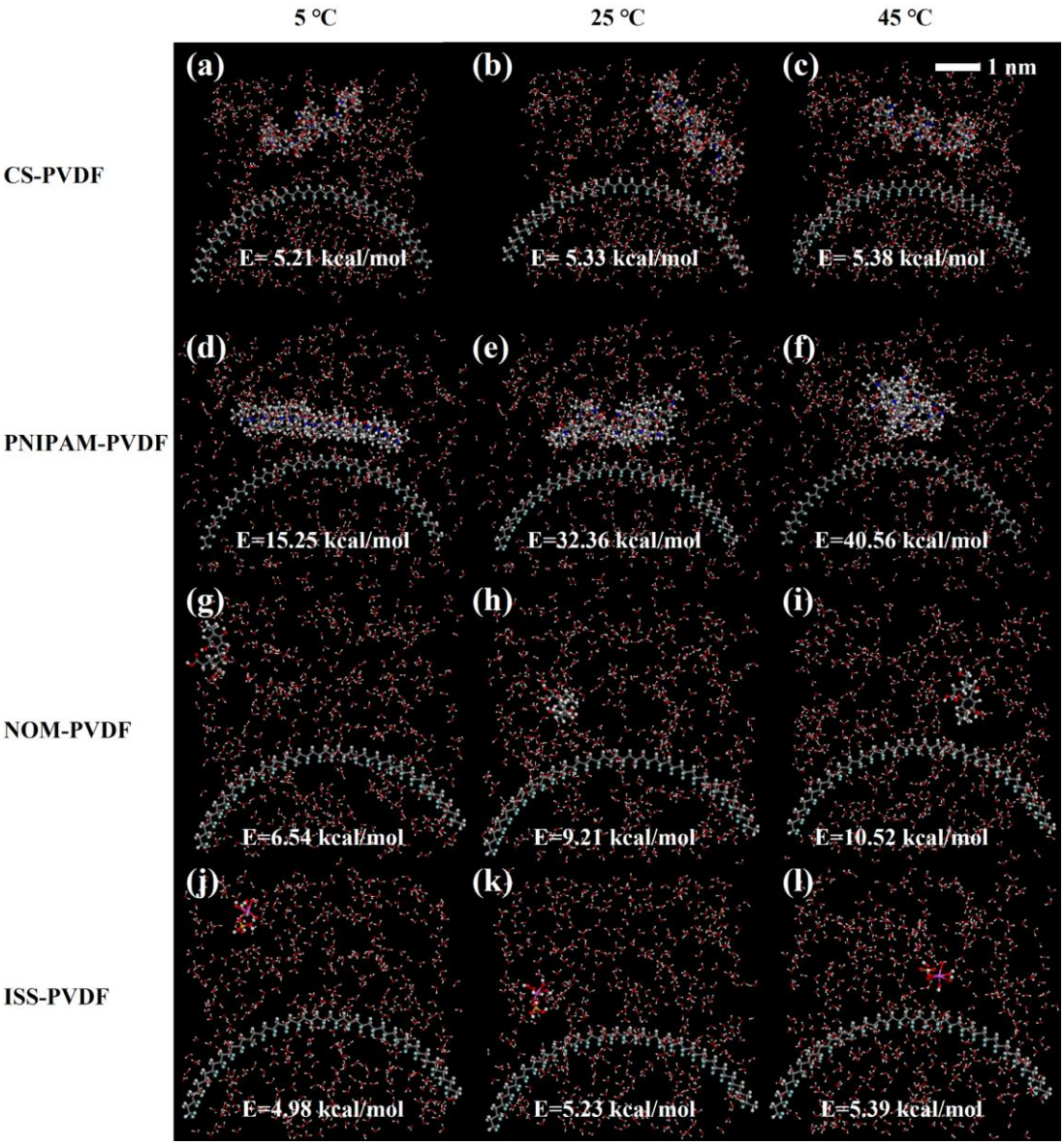


Fig. 5. Optimized structures and corresponding binding energies of different complexes formed between PVDF and various components (a-c: chitosan backbone; d-f: PNIPAM chain; g-i: representative NOM fragment; j-l: representative ISS fragment) in water at (a, d, g, and j) 5 ^{o}C, (b, e, h, and k) 25 ^{o}C, and (c, f, i, and l) 45 ^{o}C.

Figure 6

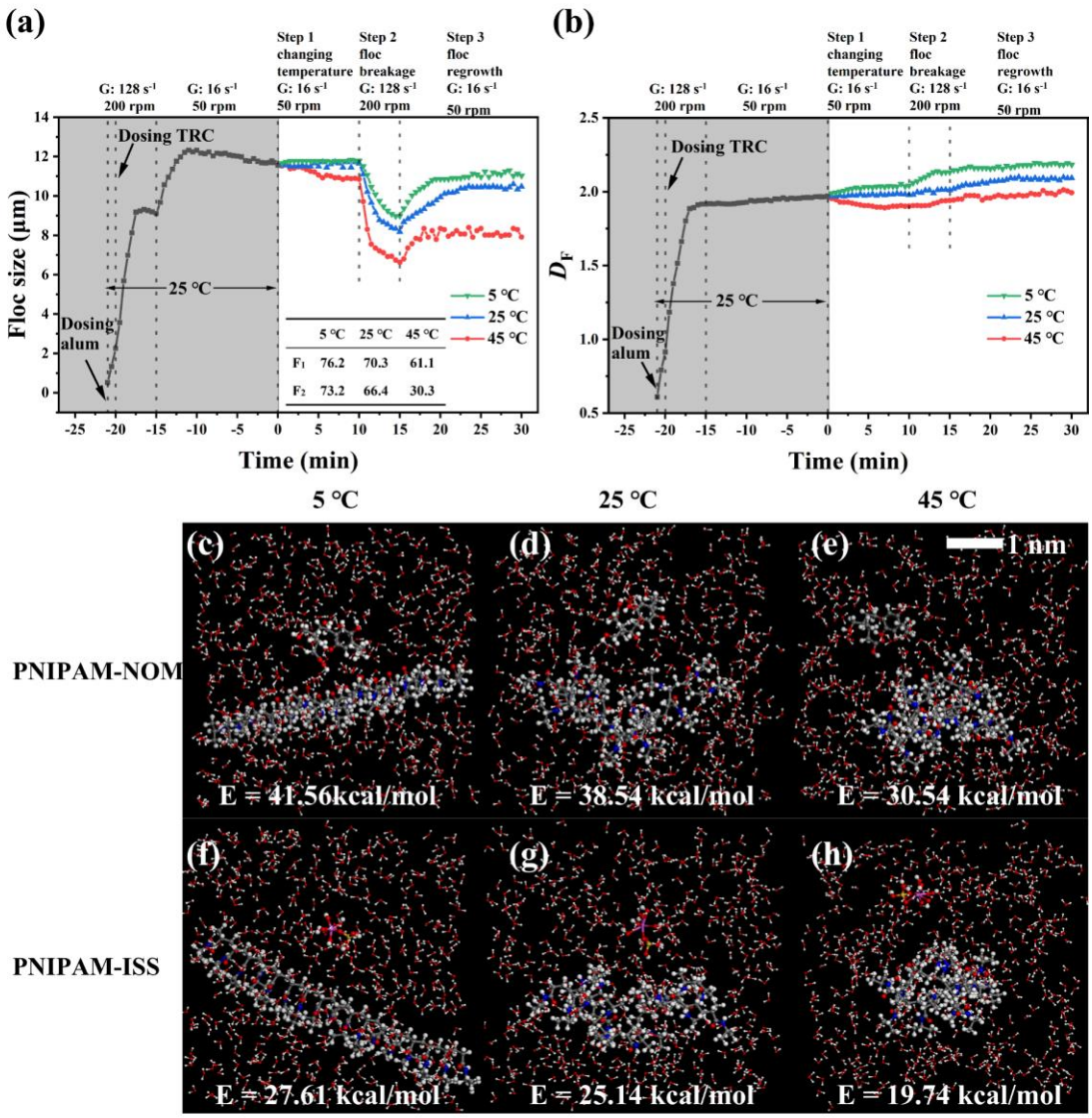


Fig. 6. (a and b) Real-time variations of (a) floc size and (b) D_F at different temperatures and velocity gradients; (c-h) Optimized structures and corresponding binding energies of different complexes formed between PNIPAM chain and various components ((c-e) representative NOM fragment; (f-h) representative ISS fragment) at (c and f) 5 ºC, (d and g) 25 ºC, and (e and h) 45 ºC.

Click here to access/download
Electronic Supplementary Material (for online publication only)
Supporting Information R (clear version).docx